Li^+ Ion Insertion in TiO_2 (Anatase). 2. Voltammetry on Nanoporous Films

Henrik Lindström, Sven Södergren, Anita Solbrand, Håkan Rensmo, Johan Hjelm, Anders Hagfeldt,* and Sten-Eric Lindquist*

Department of Physical Chemistry, University of Uppsala, Box 532, S-75121, Uppsala, Sweden

Received: February 6, 1997; In Final Form: July 9, 1997[⊗]

Electrochemical properties of Li^+ ion insertion in nanoporous TiO_2 (anatase) electrodes were studied by voltammetry. Linear and cyclic potential scans were recorded as a function of electrolyte concentration, film thickness, and temperature. The currents were directly proportional to the inner electrode area of the electrodes. The reduction of Ti^{4+} and oxidation of Ti^{3+} are sluggish and follows irreversible kinetics. The standard rate constant was $(3.5 \pm 0.5) \times 10^{-10}$ cm/s. The transfer coefficient was close to 0.5, indicating that the potential drop appears mainly across the Helmholtz layer. The capacitive currents govern largely the shape of the $i-v$ curves, except within a region near the peak potential where diffusion-limited insertion and extraction of Li^+ ions in the anatase lattice are dominating. The diffusion coefficient at 25 °C in the nanoporous structure was approximately 2×10^{-17} cm^2/s for insertion and 4×10^{-17} cm^2/s for extraction. The activation energy was 0.4 eV for insertion and 0.5 eV for extraction. The maximum obtained mole fraction of Li^+ in Li_xTiO_2 was $x = 0.47$.

1. Introduction

The electrochemical process in which cations are incorporated into the bulk lattice of a solid electrode is termed ion intercalation or ion insertion. Voltammetry is frequently used for electrochemical characterisation of ion-insertion electrodes.[1] Specifically, for nanoporous anatase, it has been combined with BET to investigate ion insertion, capacitance, and the effect of inner electrode area[2,3] or used in spectroelectrochemistry to determine flat-band potentials.[4] Diffusion-controlled H^+ insertion,[5] fractal dimension, and diffusion constant for Li^+ insertion[6] in nanoporous anatase have also been reported.

In part 1, chronoamperometry was used to compare lithium insertion in nanoporous electrodes and compact CVD samples of TiO_2 (anatase). The present paper aims at the electrochemical properties of lithium intercalation in nanoporous anatase that can be obtained from voltammetry.

2. Experimental Section

Materials and Apparatus. The details concerning the experimental setup, the preparation and characterization of the nanoporous (NP) electrodes, and the chemicals used are identical with those described in part 1. The inner area of the sintered nanoporous samples was determined by the equation (see part 1 and ref 3)

$$A_{tot} = 3V_{tot}(1 - P)/r \quad (1)$$

where A_{tot} is the inner area of the nanoporous electrode, V_{tot} is the film volume, P (=0.63) is the porosity, and r (=4 nm) is the average radius of the anatase particles in the NP film.

Experimental Procedure. Before any measurements were performed, each freshly prepared electrode was conditioned by cycling at 20 mV/s ~20 times between 0 and −1.5 V vs Ag/AgCl, to remove trace water[2] from the surface of the electrodes. The first scan yielded typically an extraction/insertion charge ratio of 97−99%. The subsequent scans yielded ratios above 99%. A Pt electrode was used in situ in the electrolyte (2 M $LiClO_4$ in acetonitrile) as an indicator of the relative water content using the same scan rate and voltage limits as above. It was found that a background current at this electrode (mainly capacitive, no redox peaks) of a few $\mu A/cm^2$ gave excellent insertion/extraction charge ratio in the TiO_2. Cathodic LSV curves were collected by sweeping the potential from 0 to −1.5 V after conditioning the electrode at 0 V for 10 min. The anodic scan was performed from −1.5 to 0 V and was collected after keeping the working electrode at −1.5 V for 10 min. It was found that the shape of the anodic LSV curve did not change significantly after a waiting time of only 5 min at this potential.

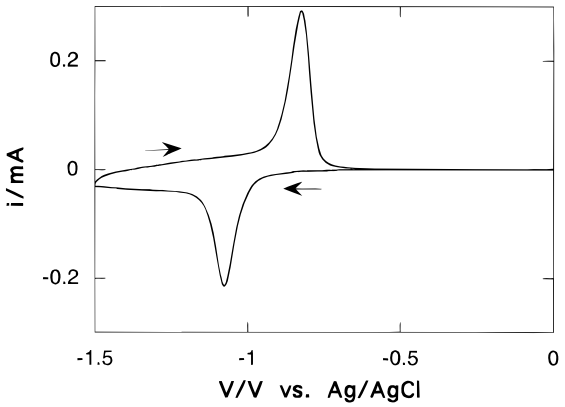

Figure 1. Cyclic voltammogram at 0.1 mV/s. Film thickness $d = 4.20$ μm. $T = 25$ °C.

3. Results and Discussion

Insertion/Extraction Charge Ratio. Figure 1 shows a cyclic voltammogram at 0.1 mV/s, with film thickness $d = 4.20$ μm. The formal potential is −0.97 V as estimated from the center between the peak potentials. The ratio between the extracted and inserted charge is 99.1%, which is higher than the previously reported value[2] of 96%. The high ratio is ascribed to the low concentration of electron acceptors in the electrolyte. The mole fraction of inserted lithium corresponds to 0.47, in agreement with earlier reports. The useful potential range for organic electrolytes permits in general maximum mole fractions of lithium in anatase of around 0.5.[2,3,7,8]

* Authors to whom correspondence should be addressed.
[⊗] Abstract published in *Advance ACS Abstracts,* August 15, 1997.

S1089-5647(97)00490-2 CCC: $14.00

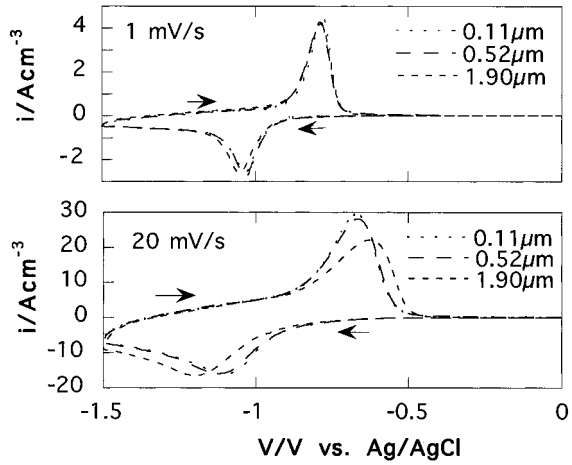

Figure 2. Comparison of the LSV curves for electrodes of different thicknesses at 1 and 20 mV/s. The currents are normalized with respect to the electrode volume. $T = 45$ °C.

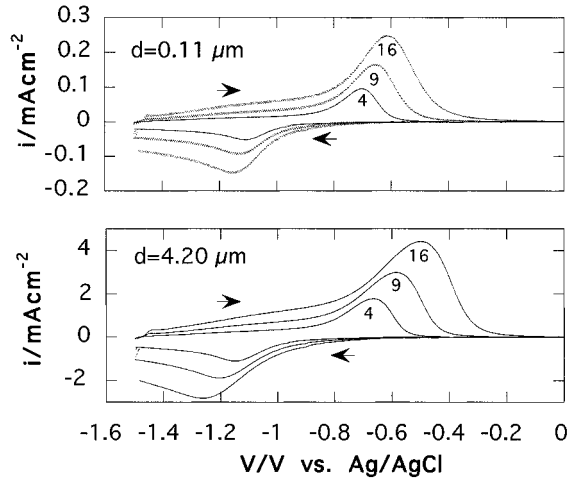

Figure 3. LSV curves at different scan rates of 4, 9, and 16 mV/s. $T = 30$ °C.

Effect of Electrode Thickness. Figure 2 shows cyclic voltammograms at two different scan rates (1 and 20 mV/s) for electrodes of different thicknesses (0.11, 0.52, and 1.90 μm). The redox currents are normalized with respect to electrode volume instead of projected area. Figure 2a shows that the $i-v$ curves for all thicknesses coincide at 1 mV/s. At 20 mV/s, in Figure 2b, the $i-v$ curve for the 1.90 μm film deviates from the other electrodes exhibiting the lowest current per volume unit.

The conclusion from Figure 2 is that the entire inner surface of the electrode is homogeneously electroactive at lower scan rates and for thinner films. This means that the electrical potential at the surface of the particles is homogeneous throughout the whole network and corresponds to that desired by the potentiostat. Additionally, the transport of electrons through the network is fast compared to the duration of the experiment at scan rates higher than 20 mV/s, especially for electrodes thinner than 1 μm. At scan rates higher than 20 mV/s and for films thicker than 1 μm (Figure 2b), the surface potential of the grains is a function of the distance from the back contact. This is due to the potential drop across the network of particles and will be discussed further below.

Effect of Scan Rate. Figure 3 displays cathodic and anodic LSV curves as a function of scan rate for two electrodes of different thicknesses, 0.11 (a) and 4.20 μm (b). Large capacitive effects are distinguished between -1.5 and -0.8 V on the anodic scans. However, it is difficult to visually resolve the charging currents on the cathodic scans. Capacitive effects are discussed further below. The peak split increases when the scan rate is increased. The peak split is slightly larger for the thicker electrode except at the lowest scan rates (see also Figure 2). The integrated charge from 0 V up to the cathodic peak at -1.1 V, in the 4 mV/s scan, corresponds to a mole fraction of $x = 0.08$ for both electrodes.

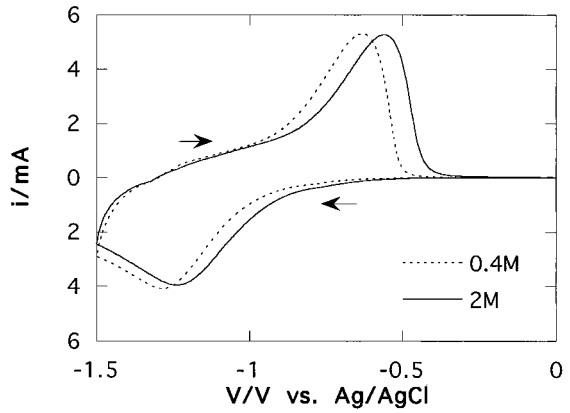

Figure 4. Comparison of cyclic voltammograms (20 mV/s) at different electrolyte concentrations (2 and 0.4 M). $d = 4.20$ μm; $T = 45$ °C.

Several studies show that double injection of electrons and Li^+ ions into TiO_2 (anatase) leads to the formation of Ti^{3+} states.[9,10] In light of this, we ascribe the cathodic peak in the voltammograms as due to the depletion of Ti^{4+} states at the surface of the particles. The low value of the integrated cathodic charge at 4 mV/s means that only a few atomic layers on the surface of each particle are reduced. The anodic wave corresponds to the oxidation of these states.

The peak split is much larger than for a Nernstian (fast) redox reaction, indicating (i) a potential drop in the system due to, for example, slow electron transport in the nanoporous network or transportation problems of the electrolyte in the cavities of the film or (ii) that the electrochemical reactions are sluggish and follow quasi-reversible or irreversible kinetics. These ideas are considered below.

Effect of Electrolyte Concentration. To elucidate to which extent the electrolyte in the cavities is consumed, the bulk electrolyte concentration was lowered to 0.4 M. Figure 4 shows the cyclic voltammograms (45 °C, 20 mV/s) for a 4.2 μm electrode at two different concentrations, 0.4 and 2 M. It can be seen that the curves are similar. The peak currents are independent of the concentration of Li^+ in the electrolyte, and the peak split is essentially independent of the electrolyte concentration. However, the entire $i-v$ curve is shifted to more negative potentials at lower electrolyte concentration, i.e., a Nernstian shift.

Since the peak split and peak height are unaffected by the change in electrolyte concentration, we conclude that the mass transfer of Li^+ ions and charge-compensating ClO_4^- ions in the film is sufficiently fast to support the redox process at the surface of each particle in the electrode network (at 20 mV/s). In a previous chronoamperometric study (part 1), we showed that the electrolyte in the pores of thicker films was depleted if large negative potential steps (e.g., -1.5 V) were applied. During a potential scan at 20 mV/s these problems are much smaller. Since the peak split is essentially independent of the electrolyte concentration (but rather of the film thickness), we conclude that the *difference* in peak split for the thicker and the thinner electrode in Figure 3 is caused by the potential drop in the TiO_2. This is probably due to slow electron transport in

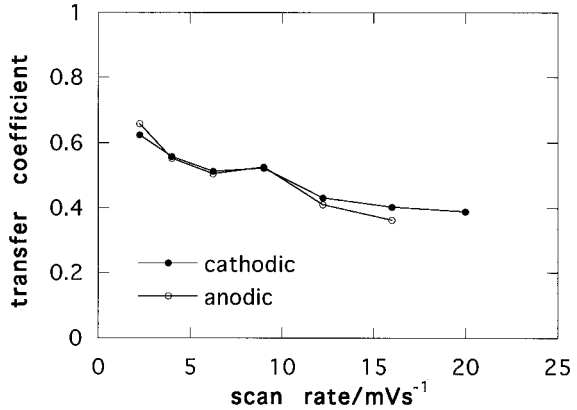

Figure 5. Transfer coefficient for different scan rates. $T = 30$ °C; $d = 0.11$ μm.

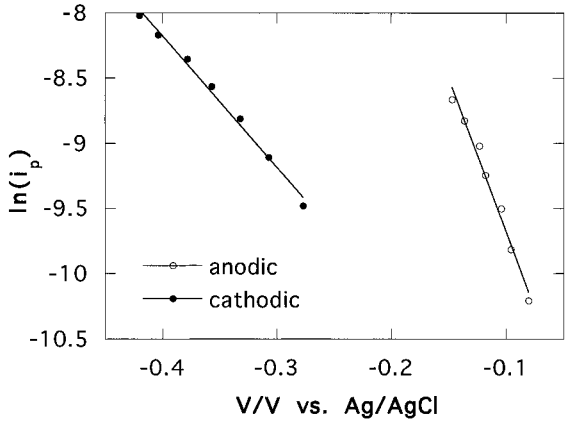

Figure 6. ln i_p as a function of $E_p - E^0$. $d = 0.11$ μm; $T = 30$ °C.

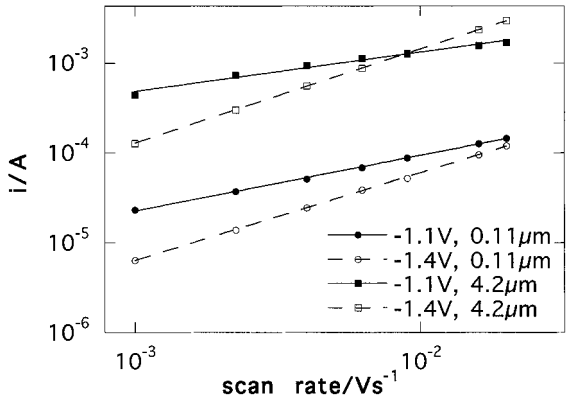

Figure 7. A log−log plot of the currents at −1.1 and −1.4 V at different scan rates. The film thicknesses are indicated in the figure. $T = 30$ °C.

the nanoporous film.[2] We conclude that the cathodic peaks in the voltammograms (at 2 and 0.4 M) are due to the depletion of Ti^{4+} states at the surface of the particles and not due to the consumption of Li^+ ions in the cavities of the film.

The onset potential of the intercalation reaction depends on the activity of the counterions in the electrolyte,[11] which is seen as a potential shift in the $i-v$ curve in Figure 4. The shift in the $i-v$ curves at different electrolyte concentrations may be compared with previous studies.[4,12] These workers used spectroelectrochemistry and extracted a specific potential (interpreted as the flat-band potential) from the absorption curves during a cathodic scan. This characteristic potential was dependent on the particular ion used, and especially for H^+ and Li^+ it shifted in a Nernstian manner with respect to the electrolyte concentration.

Transfer Coefficient. The difference between the peak potential, E_p, and the half-peak potential, $E_{p/2}$, was constant, i.e., 0.090 ± 0.005 V, for scan rates lower than 20 mV/s and for films thinner than 1 μm. A constant difference between E_p and $E_{p/2}$ at different scan rates is the characteristic feature of an irreversible electrochemical reaction, signifying that the kinetics for the reduction of Ti^{4+} and oxidation of Ti^{3+} ions at the surface is sluggish because of low exchange currents. By applying the equation for irreversible waves[13]

$$\alpha = \frac{1.857RT}{n_a F|E_p - E_{p/2}|} \qquad (2)$$

where α is the transfer coefficient, n_a is the number of electrons involved in the rate-determining step (we assume $n_a = 1$), and the other symbols have their usual meaning; α values were plotted vs scan rate (Figure 5). It can be seen that the transfer coefficient is close to 0.5 for both insertion and extraction. The values are similar to those obtained from impedance measurements on fluorinated sputtered TiO_2.[17]

Experimentally, the transfer coefficient for metals takes a value between 0.3 and 0.7.[13] A value of 0.5 means that the energy barrier for charge transfer is symmetrical. The conclusion is that the nanoporous film exhibits metallic behavior in the sense that most of the overvoltage appears across the Helmholtz layer in the electrolyte. Such behavior is often observed for semiconductors, e.g., if the density of surface states is sufficiently high or if a conducting (degenerate) overlayer is formed during the redox process.[14] Both mechanisms seem very likely, considering the insertion of Li^+ ions (doping) in the highly disordered nanoporous TiO_2.

Standard Rate Constant. The peak currents and the peak shifts were analyzed using the equation for irreversible kinetics

$$i_p = 0.227nFACk^0 \exp\left[-\left(\frac{\alpha n_a F}{RT}\right)(E_p - E^{0'})\right] \qquad (3)$$

where i_p is the peak current, C is the maximum obtainable concentration of the Ti^{3+} states (0.024 mol/cm^3 at $x = 0.5$), k^0 is the standard or intrinsic rate constant, n is the number of electrons involved in the overall electrode process, and $E^{0'}$ is the formal potential for the reaction and is estimated to −0.97 V from the center between the cathodic and anodic wave for the slowest scan used in this work (Figure 1). A plot of ln i_p vs $E_p - E^{0'}$ determined at different scan rates thus gives the values of α and k^0 (Figure 6). The obtained transfer coefficients were 0.6 (oxidation) and 0.3 (reduction), and the k^0 values were 3.8×10^{-10} cm/s (reduction) and 3.1×10^{-10} cm/s (reduction).

The transfer coefficients are similar to those in Figure 5, where eq 2 was used. The low value of the standard rate constant means that the reduction of Ti^{4+} and oxidation of Ti^{3+} states at the surface of the particles are sluggish and can be considered irreversible, which explains the strong peak shift with increasing scan rate.

Capacitive Effects. As mentioned above, substantial capacitive effects are observed for the present system. These effects were investigated by measuring how the current, i, changed with the scan rate, V, at a fixed potential. The variation of the cathodic current with scan rate at −1.1 and −1.4 V for two electrodes of different thicknesses is shown in Figure 7. The currents obey the power law, i.e.

$$i = av^b \qquad (4)$$

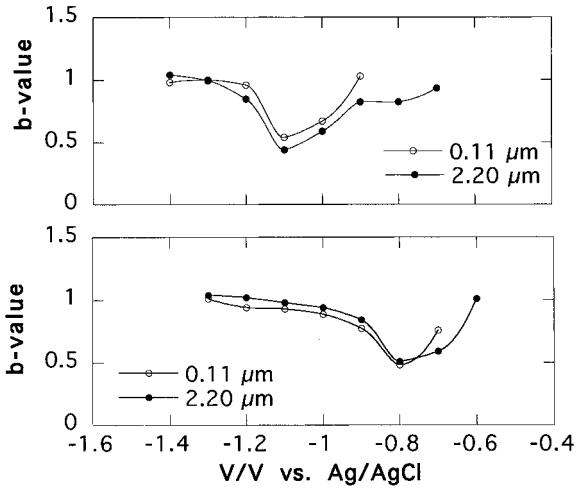

Figure 8. *b* values (see text) are plotted vs potential for cathodic (a) and anodic (b) scans. $T = 30$ °C.

where *a* and *b* are adjustable parameters. Fitting to eq 4 gives *b* values close to 0.5 at −1.1 V and 1 at −1.4 V. A more detailed picture is given in Figure 8, where the *b* values at various potentials for both the cathodic and anodic scans are shown for two electrodes of different thicknesses. The value of *b* is close to unity at all potentials, except within a small potential region around −1.1 for the cathodic scan and −0.8 for the anodic scan, where the values tend toward 0.5. Plotting the *b* values vs potential (Figure 8) reveals the close resemblance with the LSV curves in Figure 2.

The variation of the *b* values can be explained in terms of faradaic and non-faradaic currents: For a strictly diffusion-limited irreversible redox reaction, the current, *i*, at any point on the wave is expected to be proportional to the square root of the scan rate, υ, according to[13]

$$i = nFAC^*D^{1/2}\upsilon^{1/2}\left(\frac{\alpha n_a F}{RT}\right)^{1/2}\pi^{1/2}\chi(bt) \qquad (5)$$

where C^* is the surface concentration, *D* is the chemical diffusion coefficient, and *t* is the time. The χ function at any given point on the wave is a pure number. The other symbols have their usual meaning. A capacitive current, on the other hand, normally follows a linear dependence on the scan rate

$$|i_C| = AC_d\upsilon \qquad (6)$$

where i_C and C_d is the charging current and the double-layer capacitance, respectively. Hence, at higher scan rates, one can expect the currents to be dominated by capacitive charging, due to the stronger linear dependence in eq 6. The opposite will be true at lower scan rates. Naturally, in a log *i* vs log υ plot, the exponent will take a value between 0.5 (diffusion limited) and 1 (capacitive). The reason why a simple power function can fit the data quite well in Figure 7 (although the linear capacitive term becomes gradually more important with increasing scan rate) is simply that the scan rate was varied only slightly more than 1 order of magnitude. Other workers[6] analyzed the peak currents (neglecting capacitive effects) in an almost identical experiment and interpreted an exponent of 0.6, as evidence for fractality of the nanoporous TiO_2 electrode. However, this study shows that exponents between 0.5 and 1 (see Figure 7) alternatively can be associated with the influence of purely capacitive currents without invoking the concept of fractality. The fractal analysis of the porous network in high-surface-area solids have been questioned recently.[15] Previously (part 1), it was found that the amount of adsorbed ions (suggested as being Li^+) on nanoporous anatase corresponded to almost a monolayer coverage. We therefore ascribe the strong capacitive effects to the adsorption of Li^+ ions on the TiO_2 surface. We also note that the mole fraction calculated by integrating the area under a voltammogram at 20 mV/s probably is overestimated since the contributions from the charging currents are large.

Diffusion Constant. To calculate the chemical diffusion coefficient for Li^+ in the TiO_2 particles, we use the equation for an irreversible electrochemical reaction at a planar electrode,[13]

$$i_p = 0.4958nFACD^{1/2}\left(\frac{\alpha n_a F}{RT}\right)^{1/2}\upsilon^{1/2} \qquad (7)$$

where i_p is the corrected peak current in amperes (see below), *n* and n_a are taken as unity, *A* is the inner electrode area in cm^2 (from eq 1), *C* is the maximum obtainable concentration of Ti^{3+} in the lattice, i.e., 24×10^{-3} mol/cm^3 for $x = 0.5$ (see above and ref 16), *D* is the chemical diffusion constant for the Li^+ ions in cm^2/s, and the value of α is taken as 0.5. The low mole fraction obtained at 4 mV/s (0.08, see above) indicates that the diffusion of Li^+ ions is very slow, and thus a compact layer of Ti^{3+} states is built up at the surface of the particles. We assume that the diffusion layer of Ti^{3+} states is sufficiently thin compared to the particle radius such that the particle surface can be considered planar. The peak currents were plotted vs scan rate on a log−log scale and fitted to the power law (eq 3) The measurements were performed at lower scan rates (1−20 mV/s) to minimize the influence of Ohmic losses in the TiO_2. Depending on the scan rate region, the *b* values were 0.56 (between 1 and 9 mV/s) and 0.64 (if all data points between 1 and 20 mV/s were included), exhibiting a mixture between the diffusion-limited and capacitive behavior as discussed above. Attempts were made to measure the faradaic current from the base line of charging current in the LSV curves. However, the increasing peak shift at higher scan rates displaced the waves into the capacitive regions and made it difficult to visually resolve the charging current from the redox current. Nevertheless, correcting the cathodic and anodic peak currents by a capacitance of 90 and 120 $\mu F/cm^2$, respectively, gave values for *b* of 0.50 ± 0.04, independent of the scan rate or electrode thickness. The formula used was

$$i_p = i_{p,obs} - AC_d\upsilon \qquad (8)$$

where i_p is the corrected peak current, $i_{p,obs}$ is the measured peak current, *A* is the inner electrode area, and C_d and υ are the Helmholtz capacitance and scan rate, respectively. Figure 9 shows the corrected peak currents vs the square root of the scan rate for two electrodes of different thicknesses. The slopes from Figure 9 together with eq 6 give diffusion constants for Li^+ insertion of 2×10^{-17} cm^2/s (0.11 μm electrode) and 1×10^{-17} cm^2/s (4.2 μm electrode). The corresponding values for Li^+ extraction were 7×10^{-17} cm^2/s (0.11 μm) and 4×10^{-17} cm^2/s (4.2 μm). The obtained values agree with diffusion coefficients from chronoamperometric experiments (part 1) and XPS measurements[9] on nanoporous TiO_2 electrodes. We conclude that both insertion and extraction are limited by Li^+ ion diffusion in the TiO_2 particles.

Previously, the diffusion constant for Li^+ ion insertion in a nanoporous anatase electrode (roughness factor 800) was determined to 10^{-8} cm^2/s from a voltammogram.[6] These workers applied the Randles−Sevcik equation for reversible kinetics,[13] which differs from eq 7 by a factor of 0.90 if the

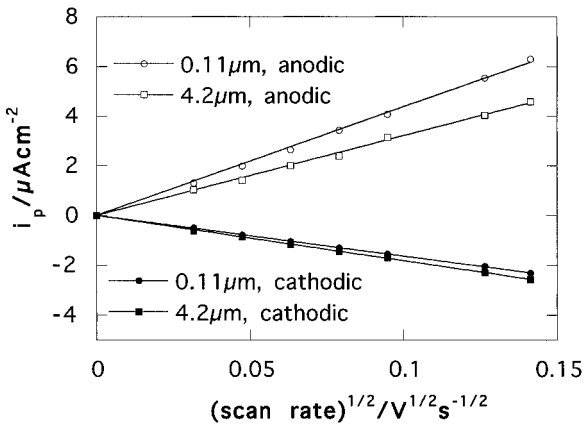

Figure 9. Corrected cathodic and anodic peak currents are plotted vs the square root of the scan rate. $T = 30$ °C.

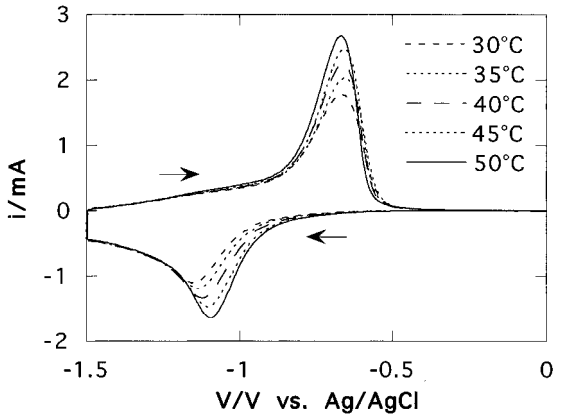

Figure 10. Temperature dependence of the LSV curves (4 mV/s). $d = 4.20$ μm.

αn_a term in eq 7 is set equal to unity. In contrast to this study, the outer electrode area (1 cm^2) and the electrolyte concentration, 1 M, i.e., 1×10^{-3} mol/cm^3, was used to calculate D. Thus, their diffusion coefficient is roughly $(800 \times 24)^2 \approx 4 \times 10^8$ times higher compared to this study (due to the square dependence in eq 8).

Effect of Temperature. Figure 10 shows the cathodic and anodic LSV curves (4 mV/s) at different temperatures for a 4.2 μm electrode. It can be seen that the peak currents depend strongly on the temperature. The magnitude of the capacitive current between -1.2 and -1.5 V (cathodic scan) and between -1.5 and -0.9 V (anodic scan) is essentially independent of the temperature. The peak split is decreased at higher temperatures.

The observations supports the view that the redox peaks are due to the diffusion-controlled depletion of Ti^{4+} or Ti^{3+} at the surface of the particles. The speed of reduction of Ti^{4+} and oxidation of Ti^{3+} states depends on the diffusion of Li^+ ions in the lattice which is a thermally activated process. The capacitive currents arise due to the continuous reorganization of the Helmholtz layer at the electrode surface when the potential is swept linearly. The temperature dependence of this non-faradaic process is expected to differ significantly from that of the diffusion-controlled redox process. The decrease in peak split can be explained by considering that the reduction of Ti^{4+} and oxidation of Ti^{3+} in the nanoporous TiO_2 network are kinetically hindered. The kinetics are more facile at higher temperatures, giving rise to a depletion peak at an earlier stage in the potential sweep.

Activation Energy. The cathodic and anodic peak currents were recorded vs scan rate (1 and 20 mV) at five temperatures.

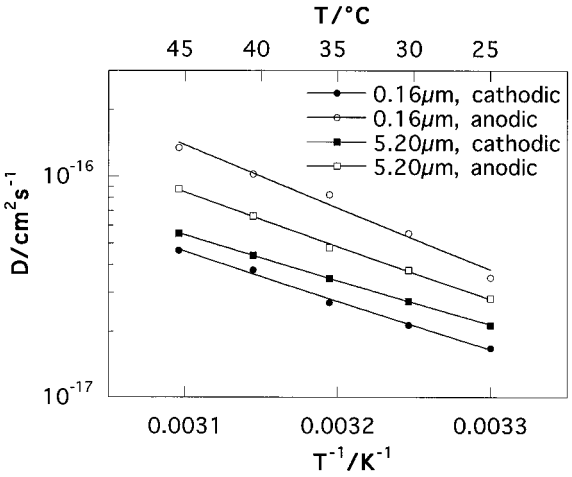

Figure 11. Relation of the logarithm of the chemical diffusion coefficient to inverse temperature.

By calculating the chemical diffusion coefficients at each temperature from eq 7, the activation energy could be determined by the relation

$$D = D_0 e^{-E_a/kT} \tag{9}$$

where D_0 is the preexponential factor, E_a is the activation energy, k is Boltzmann's constant, and T is the absolute temperature. Figure 11 shows a logarithmic plot of D vs $1/T$ for two electrodes of different thicknesses. The activation energy for insertion was 0.39 eV (0.13 μm) and 0.43 eV (4.2 μm). The corresponding values for extraction was 0.47 eV (0.13 μm) and 0.54 eV (4.2 μm).

The values are similar to those obtained from chronoamperometry (part 1) and from impedance measurements on sputtered fluorinated TiO_2 samples.[17]

4. Conclusions

The redox properties associated with Li^+ intercalation in nanoporous TiO_2 electrodes were examined by voltammetry. The currents were linearly proportional to the inner electrode area rather than to the back contact area, and under certain experimental conditions, the potential drop across the nanoporous network was negligible. The transfer coefficient was close to 0.5 for both insertion and extraction. Thus, the nanoporous anatase film exhibit metallic behavior in the sense that the potential drop appears mainly across the Helmholtz layer; i.e., the potential drop within the particles is small. The standard rate constant was $\sim 10^{-10}$ cm/s, giving rise to irreversible behavior. Consequently, large overpotentials are required to reach the limiting currents. LSV measurements yielded diffusion coefficients on the order 10^{-17} cm^2/s. The values are of the same order as those obtained in a previous study and confirm that the solid state diffusion of lithium in the particles is very slow. At higher scan rates or for thicker films the insertion and extraction were additionally limited by the potential drop in the TiO_2. The capacitive effects could be resolved from the diffusion-limited faradaic reactions by analyzing the currents in the $i-v$ curves at different potentials or by changing the temperature of the electrolyte.

Acknowledgment. The authors thank Fariba, Maria, and Susann for all help and stimulating discussions. This work was supported by the Swedish Research Council for Engineering

Sciences (TFR), the Commission of the European Community Joule II program, and the Swedish National Research Council (NFR).

References and Notes

(1) Granqvist, C. G. *Handbook of Inorganic Electrochromic Materials*; Elsevier Science: Amsterdam, 1995.

(2) Kavan, L.; Kratochilová, K.; Grätzel, M. *J. Electroanal. Chem.* **1995**, *394*, 93−102.

(3) Kavan, L.; Grätzel, M.; Rathousky, J.; Zukal, A. *J. Electrochem. Soc.* **1996**, *143*, 394−400.

(4) Redmond, G.; Fitzmaurice, D. *J. Phys. Chem.* **1993**, *97*, 1246−1430.

(5) Cao, F.; Oskam, G.; Searson, C.; Stipkala, J. M.; Heimer, T. A.; Meyer, G. J. *J. Phys. Chem.* **1995**, *99*, 11974−11980.

(6) Stromme, M.; Niklasson, G. A.; Granqvist, C. G. *Solid State Commun.* **1995**, *96*, 151−154.

(7) Murphy, D. W.; Greenblatt, M.; Zahurak, S. M.; Cava, R. J.; Waszczak, J. V.; Hull, G. W.; Hutton, R. S. *Rev. Chim. Miner.* **1982**, *19*, 441.

(8) Zachau-Christiansen, B.; West, T.; Jacobsen, T. a. A. S. *Solid State Ionics* **1988**, *28*−30, 1176.

(9) Södergren, S.; Rensmo, H.; Lindström, H.; Hagfeldt, A.; Lindquist, S.-E.; Siegbahn, H. *J. Phys. Chem. B* **1997**, *101*, 7710−7716.

(10) Stashans, A.; Lunell, S.; Bergström, R.; Hagfeldt, A.; Lindquist, S.-E. *Phys. Rev. B* **1996**, *53*.

(11) Hitchman, M. L. *J. Electroanal. Chem.* **1977**, *85*, 135−144.

(12) Rothenberger, G.; Fitzmaurice, D.; Grätzel, M. *J. Phys. Chem.* **1992**, *96*, 5983−5986.

(13) Bard, A. J.; Faulkner, L. R. *Electrochemical Methods: Fundamentals and Applications*; John Wiley & Sons: New York, 1980.

(14) Morrison, S. R. *Electrochemistry at Semiconductor and Oxidized Metal Electrodes*; Plenum Press: New York, 1980.

(15) Curtis Conner, W.; Bennet, C. O. *J. Chem. Soc., Faraday Trans.* **1993**, *89*, 4109−4114.

(16) Kavan, L.; Grätzel, M.; Gilbert, S. E.; Klemenz, C.; Scheel, H. J. *J. Am. Chem. Soc.* **1996**, *118*, 6716−6723.

(17) Stromme, M.; Gutarra, A.; Niklasson, G.; Granqvist, C. G. *J. Appl. Phys.* **1995**, *79*, 3749−3757.